

Article

Improved Whale Optimization Algorithm for Solving Microgrid Operations Planning Problems

Yixing Liu , Shaowen Yang, Dongjie Li and Shouming Zhang *

Faculty of Information Engineering and Automation, Kunming University of Science and Technology, Kunming 650500, China

* Correspondence: zhangsm@stu.kust.edu.cn

Abstract: Microgrid operations planning is one of the keys to ensuring the safe and efficient outputs of distributed energy resources (DERs) and the stable operation of a power system in a microgrid (MG). In this study, for the symmetry in renewable energy and microgrid systems, and coordinated control based on a storage battery system, an MG dispatching model with DER conditions and integrated costs is established in grid-connected mode, on the basis of MG operation costs, interaction costs, and pollutant emissions costs. Moreover, an optimization objective for minimizing integrated costs is established. Therefore, based on the original whale optimization algorithm (WOA), an improved whale optimization algorithm (IWOA) with adaptive weight strategy and Levy flight trajectory is proposed in this paper, to solve the optimal operations planning problem of MGs. Finally, in computing comparisons with methods such as the genetic algorithm (GA), particle swarm algorithm (PSO), WOA, wild horse optimizer (WHO), and enhanced whale optimization algorithm (EWOA), the results show that the IWOA computation had lower integrated costs and higher operational efficiency. Moreover, it is verified that the IWOA performed better in solving the MG operations planning problem.

Keywords: adaptive weight strategy; Levy flight trajectory; whale optimization algorithm; microgrid; system operations planning



check for updates

Citation: Liu, Y.; Yang, S.; Li, D.; Zhang, S. Improved Whale Optimization Algorithm for Solving Microgrid Operations Planning Problems. *Symmetry* **2023**, *15*, 36. <https://doi.org/10.3390/sym15010036>

Academic Editors: Alfredo Alcayde and Raúl Baños Navarro

Received: 20 November 2022

Revised: 5 December 2022

Accepted: 18 December 2022

Published: 23 December 2022



Copyright: © 2022 by the authors. Licensee MDPI, Basel, Switzerland. This article is an open access article distributed under the terms and conditions of the Creative Commons Attribution (CC BY) license (<https://creativecommons.org/licenses/by/4.0/>).

1. Introduction

In recent years, along with the increasingly severe fossil fuel energy crisis and environmental pollution pressure, clean energy generation has become one of the priorities for future development in various countries. While vigorously developing wind, solar, and other renewable energy sources as important power sources, their inherent random and intermittent energy generation also introduces problems, such as excessive system power fluctuations, insufficient scheduling capacity, and power quality disturbances [1–4]. To effectively use primary energy such as wind and solar energy, microgrid technology has come into being, which consists of DERs, energy storage systems, loads, and monitoring [5,6]. A microgrid has independent power generation, transmission, and distribution capabilities, and can operate either in grid-connected or islanded mode, with regional energy balance and strong dispatchability [7,8]. Microgrid technology can not only improve the quality of the power supply in remote areas, such as mountainous areas and islands but can also effectively prevent large-scale power outages that are caused by accidents and disasters [9,10]. However, with the widespread integration of clean energy power generation technology, the composition and structure of the power supply will become more complex and diversified, posing challenges to the reactive power balance and power quality of the entire power generation system [11].

Optimal operations planning of a microgrid power supply system will bring better economy, security, and reliability, as well as lower pollution [12]. For a large grid (LG), traditional optimization methods are not effective, due to the impact of their more

complex calculations [13]. Therefore, the emergence of meta-heuristic algorithms can effectively solve these traditional optimization method problems for LG systems [14,15]. Most meta-heuristic algorithms are inspired by physical phenomena or natural species and are designed by related scholars [16]. Meta-heuristic algorithms have simple parameters and convenient implementation, are easy to understand and can solve related problems using iterative procedures that simulate the evolution of natural processes for objective optimization [12].

Many experts and scholars have used meta-heuristic algorithms for solving microgrid operations planning problems. Bahmani et al. [17] noticed a significant use of renewable energy sources (RESs) in microgrids and, therefore, a dramatic increase in the use of energy storage systems. For this reason, they introduced a bat algorithm to perform a corrective strategy for minimum-cost dispatch. Mohamed et al. [18] noticed an application of permanent magnet synchronous generators (PMSGs) in advanced wind systems. They introduced maximum power point tracking (MPPT) control methods and the latest trends in PMSG wind system components to assist researchers in pushing the grid integration in modern power systems. Abbasi et al. [19] used the flower pollination algorithm (FPA) in demand side management (DSM) to schedule appliances to meet consumer load demands. In addition, they emphasized reducing the peak-to-mean ratio and the cost of electricity. Zhang et al. [20] introduced a method that helps to schedule microgrid resources. For this purpose, they proposed a hybrid optimization algorithm. Muhammad et al. [21] introduced an architecture with integrated RESs. This approach classified different users, and assigned priority according to energy demand, which reduced the costs of electricity consumption and improved user comfort. Sukumar et al. [22] introduced a mixed-mode energy management strategy, and proposed a battery selection method to reduce the costs of microgrid operation. Askarzadeh et al. [23] used a memory-based genetic algorithm (MGA) to optimize an islanded microgrid system and reduce the costs of generating electricity from the islanded microgrid system. Gholami et al. [24] used an improved personal optimal particle swarm optimization algorithm to minimize the generation costs of an isolated microgrid system that contained three wind motors, two photovoltaic systems, and a combined heat and power cogeneration (CHP) system that was connected to an IEEE 37 node feeder. Nadimi-Shahraki et al. [25] studied the optimal power flow (OPF) problem. They proposed an effective hybridizing of WOA and a modified moth-flame optimization algorithm (MFO) named WMFO to reduce the costs of ten different OPF problems. Lahon et al. [26–28] studied the optimal power dispatch for the cooperative operation of multiple coupled microgrids, where a contribution level-based scheme was considered, to provide power exchange between microgrids. The expected profit of each microgrid was maximized by stimulating the energy transfer between the microgrids. Trivedi et al. [29] implemented an internal search algorithm (ISA) to perform penalty factor-based combined economic emission dispatch (CEED), on a three-unit microgrid system consisting of wind motors and photovoltaic systems. Motevasel et al. [30] proposed a microgrid system with reduced net emissions and generation costs to enhance system stability, but they did not consider a mechanism to reduce PAR. Tahmasebi et al. [31] proposed an optimal operations management model for a stand-alone microgrid that considered demand response (DRP). They used a whale optimization algorithm to minimize the operating and emissions costs, arguing the importance of demand response systems (DRPS). Khodaei et al. [32] introduced the concept of a temporary microgrid, proposed a new optimal dispatch model, and demonstrated the advantages of this new microgrid. The implications of this concept were further used in planning the next generation of smart and sustainable integrated grids [33].

Current research on the optimal operations planning strategy of microgrids focuses on improving the efficiency of renewable energy use, and on reducing the operations and pollutant emissions costs. The research on reducing the interaction with a large grid in grid-connected mode is insufficient. Under grid-connected operation, reducing the amount of microgrid interaction with a larger grid can improve the robustness and safety of the

microgrid power supply. Moreover, meta-heuristic algorithms mainly feature low accuracy and slow response in solving optimal microgrid operations planning problems. Therefore, to increase the proportion of clean energy generation, reduce the degree of interaction between the microgrid and large grid, and ensure the security between DERs and the stable operation of the whole power system, this paper proposes an improved whale optimization algorithm (IWOA), based on adaptive weight strategy and Levy flight trajectory. It was used to solve the optimal operations planning problem of a grid-connected microgrid under the optimal output condition of DERs. Aiming at the economic operation and environmental protection of the microgrid, to ensure the symmetry in renewable energy and microgrid systems, the mathematical model and optimization objective function of each power generation unit in the microgrid were established by considering the differences between influencing factors, such as load demand, time-sharing tariff, and pollutant emissions.

In the next sections, the objective function and DERs generating model are established for grid-connected microgrid operations planning problems. Moreover, WOA's location update equations are introduced, and based on this, the location update equations of IWOA are proposed by introducing an adaptive weight strategy and Levy flight trajectory to enhance WOA's global search capability. Finally, on the basis of grid-connected microgrid operations data, using IWOA to solve the objective function to obtain the minimized operation cost and ensure the symmetry in renewable energy and microgrid systems. To verify the effectiveness of IWOA, the result is also compared with the results solved by GA, PSO, WHO, WOA, and EWOA.

2. A Microgrid Optimizing Model

The grid-connected microgrid structure consists of two major parts: the power supply system and the loads, where the power supply system consists of DERs that include wind turbines (WTs), photovoltaics (PVs), diesel engines (DEs), fuel cells (FCs), and batteries (BATs). In addition, a microgrid will interact with a large grid. Figure 1 shows a typical structure of a grid-connected microgrid.

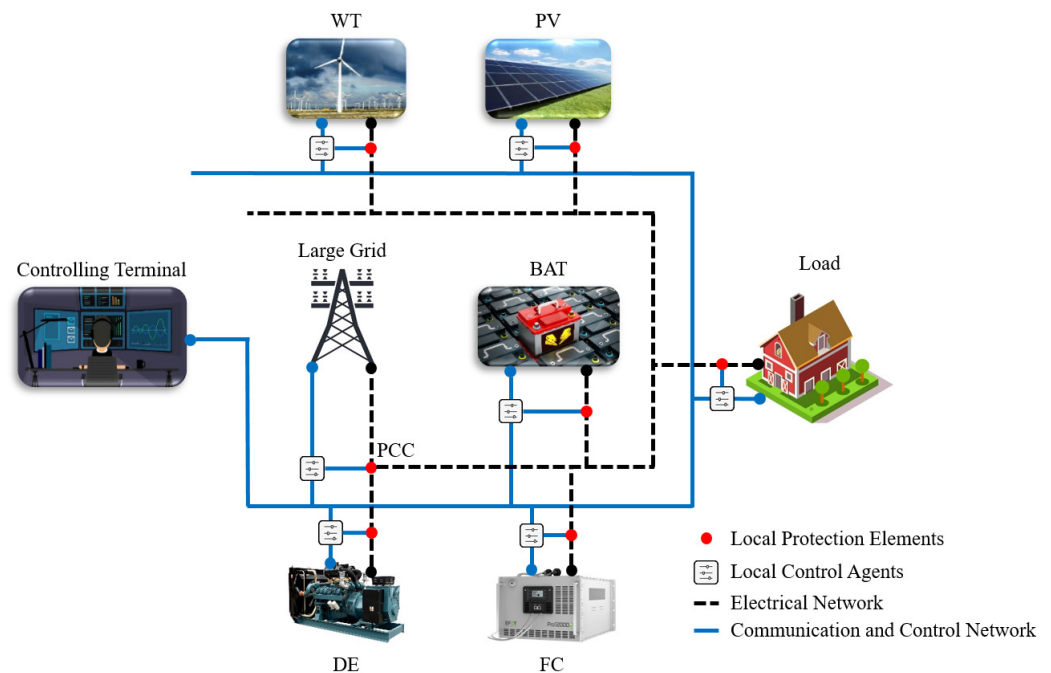


Figure 1. A typical structure of a grid-connected microgrid.

A grid-connected microgrid needs to meet the dynamic power balance, and ensure the stable operation of the power supply system. Based on satisfying this condition, this study set its research objectives to increase the proportion of RES generation, reduce the

degree of interaction between the microgrid and the large grid, and reduce the microgrid operations costs and pollutant emissions costs. The relevant system models and objective functions are described in the following subsections.

2.1. Objective Function

The objective of optimal microgrid operations planning in grid-connected mode is to minimize the integrated costs, including the microgrid operations costs and pollutant emission costs, as shown in Equation (1):

$$\min F = \omega_1 \cdot f_1 + \omega_2 \cdot f_2 \quad (1)$$

where F is the integrated cost of the microgrid, f_1 is the operation cost function, and f_2 is the pollutant emissions cost function. ω_1 and ω_2 are the weighting coefficients of each function, which specify the optimization priority. The operation cost function f_1 is defined by Equations (2) and (3). The pollutant emissions cost f_2 is defined by Equations (4) and (5).

f_1 is composed of the operation costs of each DER and the costs of the microgrid interacting with the larger grid. Its mathematical expressions are shown in Equations (2) and (3):

$$f_1 = \sum_t^T (C_{grid}(t) + C_{BE}(t) + C_{WT}(t) + C_{PV}(t) + C_{DE}(t) + C_{FC}(t)) \quad (2)$$

$$\begin{cases} C_{grid}(t) = C_{buy}(t) + C_{sell}(t) \\ C_{buy}(t) = c_b(t)P_b(t) \\ C_{sell}(t) = c_s(t)P_s(t) \end{cases} \quad (3)$$

where $P_b(t)$ and $P_s(t)$ are the power that is purchased and sold by the microgrid to the large grid at time t , respectively. $C_{buy}(t)$ and $C_{sell}(t)$ are the costs of electricity purchased and sold by the microgrid to the large grid at time t , respectively. $c_b(t)$ and $c_s(t)$ are the prices of electricity purchased and sold by the microgrid to the large grid at time t , respectively. An MG cycle dispatching model with DER conditions and integrated costs was established.

f_2 is generated by the penalty costs that are caused by polluting the environment. During microgrid operation, the generator units that rely on non-renewable energy sources produce a certain amount of pollutants, including CO_2 , SO_2 , CO , and NO_x . f_2 is defined according to Equation (4). Equation (5) determines the average cost of each type of pollutant that is emitted by DEs and FCs.

$$f_2 = \sum_t^T (C_{DE.en}(t) + C_{FC.en}(t)) \quad (4)$$

$$\begin{cases} C_{DE.en}(t) = (E_{\text{CO}_2}^{DE} + E_{\text{SO}_2}^{DE} + E_{\text{NO}_x}^{DE} + E_{\text{CO}}^{DE}) \cdot P_{DE}(t) \\ C_{FC.en}(t) = (E_{\text{CO}_2}^{FC} + E_{\text{SO}_2}^{FC} + E_{\text{NO}_x}^{FC} + E_{\text{CO}}^{FC}) \cdot P_{FC}(t) \end{cases} \quad (5)$$

where $C_{DE.en}(t)$ is the pollutant emissions cost of a DE at time t , and $C_{FC.en}(t)$ is the pollutant emissions cost of an FC at time t . $P_{DE}(t)$ and $P_{FC}(t)$ are the powers that are output by the DE and the FC, respectively, at time t .

2.2. Distributed Energy Resources Model

A WT is a power generation technology that converts mechanical energy into electrical energy via wind-driven fan blade rotation. The mathematical expression of wind turbine output power [34] is shown in Equation (6):

$$P_{WT} = \begin{cases} 0, & 0 \leq v \leq v_{ci} \\ \frac{P_r(v-v_{ci})}{v_r-v_{co}}, & v_{ci} \leq v \leq v_r \\ P_r, & v_r \leq v \leq v_{co} \\ 0, & v_{co} \leq v \end{cases} \quad (6)$$

where P_{WT} is the output power of the WT, p_r is the rated power of the WT, v is the actual wind speed, v_r is the rated wind speed, v_{ci} is the cut-in wind speed, and v_{co} is the cut-out wind speed.

A PV is a power generation technology that converts light energy directly into electricity, through the photovoltaic effect, at the semiconductor interface. The output power of a PV is affected by factors such as light intensity and the temperature of the PV panel surface, and its mathematical expression [35] is shown in Equation (7):

$$P_{PV} = P_{STC} \frac{G}{G_{STC}} [1 + \delta(T_{en} - t_{STC})] \quad (7)$$

where P_{PV} is the actual output power of the PV, and P_{STC} is the output power of the PV under standard test conditions. G is the light intensity, G_{STC} is the light intensity under standard test conditions, δ is the temperature power coefficient, T_{EN} is the ambient temperature, and T_{STC} is the temperature under standard test conditions.

A DE is a power generation technology that uses diesel fuel and a diesel engine as the prime mover to drive the generator components and generate electricity. It has the advantages of providing stable power generation, being generally free from external interference, and having high reliability. When the output power of renewable energy generation is insufficient, a DE is connected to the microgrid as a supplementary energy source to meet the load demand. The mathematical expression of its power generation cost is shown in Equation (8):

$$C_{DE.fuel} = k_1 + k_2 P_{DE} + k_3 P_{DE}^2 \quad (8)$$

where $C_{DE.fuel}$ is the fuel cost of the DE, and P_{DE} is the output power of the DE. k_1 , k_2 , and k_3 are the fuel cost coefficients.

An FC is a power generation technology that directly converts chemical energy into electrical energy without intermediate processes, i.e., no Gibbs-free energy losses. Compared with traditional fossil fuel power generation, an FC is more efficient. It produces less pollution, and the relationship between its efficiency and output power is shown in Equation (9); the mathematical expression of its power generation costs is shown in Equation (10):

$$\lambda_{FC} = -0.0023 P_{FC} + 0.6735 \quad (9)$$

$$C_{FC} = c_{FC} \cdot T_{run} \cdot \frac{1}{LHV} \sum_t \frac{P_{FC}(t)}{\lambda_{FC}(t)} \quad (10)$$

where P_{FC} is the fuel cell output power, λ_{FC} is the fuel cell power efficiency, c_{FC} is the fuel cell power cost, c_{FC} is the fuel price, T_{run} is the operation time, $P_{FC}(t)$ is the fuel cell output power at time t , and $\lambda_{FC}(t)$ is the fuel cell efficiency at time t . LHV is the low heating value of the fuel.

Storage battery system plays the role of maintaining the power supply's balance and energy buffer and is used for the coordinated control of the microgrid to regulate the symmetry in renewable energy and microgrid systems. State of charge (SOC) is an important technical index to measure the state of charge of the battery, and its mathematical expression is shown in Equation (11):

$$SOC(t) = \begin{cases} SOC(t-1) + \frac{1}{\mu^-} P_{BE}(t), P_{BE}(t) \leq 0 \\ SOC(t-1) + \mu^+ P_{BE}(t), P_{BE}(t) > 0 \end{cases} \quad (11)$$

where $SOC(t)$ is the remaining capacity of the battery at time t . $P_{BE}(t)$ is the charge and discharge power of the battery at time t ; when it is positive, it means discharge, while negative means charge. μ^+ and μ^- are the charge and discharge efficiencies, respectively.

2.3. Constraints

In designing the microgrid optimization model, which is influenced by the equipment's parameters and other factors, each power generation unit needs to meet certain constraints, to ensure that the system works stably and safely when outputting electricity.

The microgrid must meet the power balance constraints that occur during operation to ensure the normal operation of the system. The constraint expression is shown in Equation (12):

$$P_{Load}(t) = P_{grid}(t) + P_{BE}(t) + P_{WT}(t) + P_{PV}(t) + P_{DE}(t) + P_{FC}(t) \quad (12)$$

where $P_{Load}(t)$ is the load power of the microgrid at time t .

The power output of each DER in the microgrid cannot exceed its respective upper and lower limits, and its constraints are shown in Equation (13):

$$P_i^{\min} \leq P_i(t) \leq P_i^{\max} \quad (13)$$

where $P_i(t)$ is output power of the i -th controllable generator set at time t . P_i^{\max} and P_i^{\min} are the upper and lower limits of the output power of the i -th controllable generator set, respectively.

Each DER in the microgrid has a certain limit on the power increase or decrease rate, i.e., the climbing constraint. This constraint is shown in Equation (14):

$$P_i(t) - P_i(t-1) \leq p_i \Delta t \quad (14)$$

where p_i is the maximum climb rate of the i -th controllable generator unit. Δt is the increment in operation time.

There is also a limit on the microgrid interacting with the larger grid, and the constraint is shown in Equation (15):

$$P_{grid}^{\min} \leq |P_{grid}(t)| \leq P_{grid}^{\max} \quad (15)$$

where P_{grid}^{\max} and P_{grid}^{\min} are the upper and lower limits of power for the interaction between the microgrid and the large grid, respectively.

During the regular operation of a battery, there are charge and discharge power limits and capacity limits. These constraints are shown in Equation (16):

$$\begin{cases} P_{BE}^{\min} \leq P_{BE}(t) \leq P_{BE}^{\max} \\ SOC_{\min}(t) \leq SOC(t) \leq SOC_{\max}(t) \end{cases} \quad (16)$$

where P_{BE}^{\max} and P_{BE}^{\min} are the upper and lower limits of battery capacity, respectively; a positive value means that the battery is discharging, while a negative value means that the battery is charging. $SOC_{\max}(t)$ and $SOC_{\min}(t)$ indicate the upper and lower limits of the battery's capacity at time t , respectively.

3. Optimization Methods

Microgrid operations planning is a complex problem that involves optimizing the output of DERs while minimizing operation costs. Solving this problem with meta-heuristic algorithms can significantly improve the quality of solution results. This section proposes an improved whale algorithm (IWOA) based on adaptive weight and opposition-based learning.

3.1. Whale Optimization Algorithm

The whale optimization algorithm (WOA) was proposed by Mirjalili [36], it simulates the predation behavior of humpback whales, and searches for an optimal solution location based on three search mechanisms: envelope predation, bubble predation, and random search during the predation process. In the search phase, each individual searches for prey in the entire search space, which is a global search process. The better the global search capability and population diversity, the less risk there is of the algorithm falling into local convergence. In the predation phase, each individual is guided by the optimal

global individual to rapidly cluster and contract toward that individual, and search for the existence of higher-quality individuals in the local search space. At this time, the algorithm converges faster, but the search effort decreases, and the algorithm may prematurely converge to local extremes.

The assumption is that the current optimal candidate solution is the target prey location or the location closest to the target prey. After recording the optimal candidate location, other whales will approach this location using the encircling predation mechanism of the WOA. The position update formula at this time is shown in Equation (17):

$$\begin{cases} X(t_{iter} + 1) = X^*(t_{iter}) - A \cdot D \\ D = |C \cdot X^*(t_{iter}) - X(t_{iter})| \\ A = 2a \cdot r_1 - a \\ C = 2r_1 \\ a = 2 \left(1 - \frac{t_{iter}}{T_{max}}\right) \end{cases} \quad (17)$$

where $X^*(t_{iter})$ is the optimal individual of the current population, namely, the location of the optimal candidate solution; $x(t_{iter} + 1)$ is the location of the next generation population individual, and $x(t_{iter})$ is the location of the current population individual. D denotes the distance between the current population optimal individual and other individuals, A is the convergence factor, C is the oscillation factor, r_1 is a random number within $(0, 1)$, and a is the wandering factor.

In addition to encirclement predation, the local search stage uses spiral bubbles to contract and encircle prey. The whale's position is updated as it approaches its prey. This method can speed up the local search, which belongs to the bubble predation mechanism of the WOA. The position update equation at this time is shown in Equation (18):

$$\begin{cases} X(t_{iter} + 1) = D' \cdot e^{br_2} \cdot \cos(2\pi r_2) + X^*(t_{iter}) \\ D' = |X^*(t_{iter}) - X(t_{iter})| \end{cases} \quad (18)$$

where D' denotes the distance between the optimal individual of the current population and the other individuals; b is the logarithmic spiral shape coefficient, usually taken as 1; and r_2 is a random number within $[-1, 1]$.

The random search mechanism takes the value of the convergence factor A as the judgment criterion. When $|A| \geq 1$, the whale individual will deviate from the candidate solution position for the global search of the algorithm, to improve the search capability of the WOA and avoid the algorithm from falling into the local optimum. Its position update formula is shown in Equation (19):

$$\begin{cases} X(t_{iter} + 1) = X_{rand}(t_{iter}) - A \cdot D'' \\ D'' = |C \cdot X_{rand}(t_{iter}) - X(t_{iter})| \end{cases} \quad (19)$$

where $X_{rand}(t_{iter})$ is the location of a random whale individual in the current population, and d'' denotes the distance between a random individual and other individuals in the current population.

Each of the two mechanisms in the WOA local search phase has a 50% probability of occurring during the search. Therefore, let p be a random number within $(0, 1)$, add a judgment criterion into Equations (17) and (18), and synthesize Equation (19) to obtain the overall WOA location update formula, as shown in Equation (20):

$$X(t_{iter} + 1) = \begin{cases} X^*(t_{iter}) - A \cdot D, p < 0.5, |A| < 1 \\ X_{rand}(t_{iter}) - A \cdot D'', p < 0.5, |A| \geq 1 \\ D' \cdot e^{br_2} \cdot \cos(2\pi r_2) + X^*(t_{iter}), p \geq 0.5 \end{cases} \quad (20)$$

Within the set number of iterations, based on the changes in the values of p and A , the WOA uses the above three mechanisms to update the individual positions continuously, and find the position of the feasible optimal solution to complete the optimization goal and end the algorithm cycle. The WOA's flow chart is shown in Figure 2.

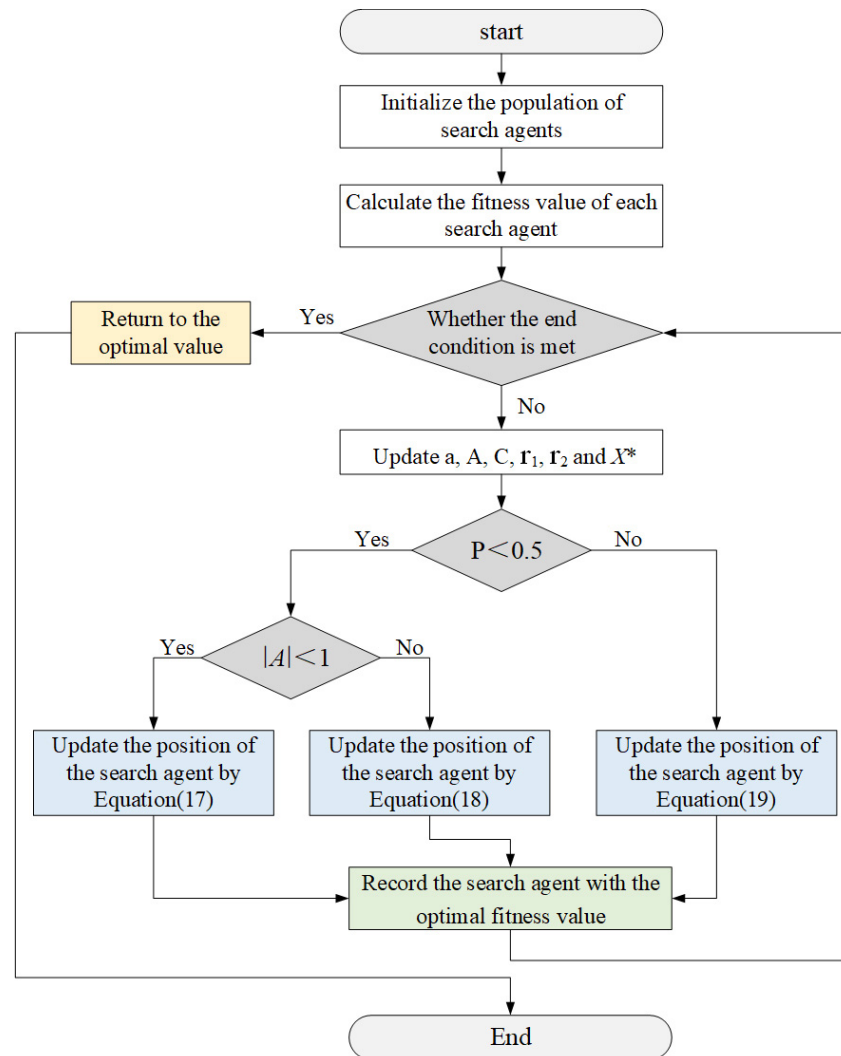


Figure 2. The WOA's flow chart.

3.2. IWOA

The touring factor a in the original WOA tends to decrease linearly in the iterative process. Inspired by previous experience [37], to make the WOA avoid the problem of prematureness when dealing with high-dimensional complex problems, and balancing the global and local search abilities, a nonlinear swimming factor formula was proposed in this paper. Its expression is shown in Equation (21):

$$a = 2 \left(1 - \left(\frac{t_{iter}}{T_{max}} \right)^3 \right) \quad (21)$$

The change curve of a 's value, before and after the improvement, is shown in Figure 3.

The change in swimming factor a determines the change in the convergence factor A , as described above, coordinating the global and local searches of the WOA. As seen in Figure 3, the improved a value is larger and decreases more slowly at the beginning, which can improve the global search performance of the algorithm. The improved a value decreases faster in the later stage, which improves the local search performance of the algorithm.

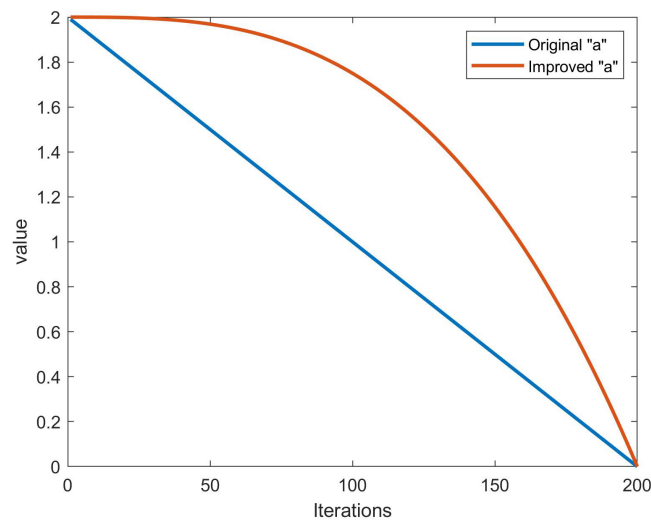


Figure 3. The value of a .

Introducing adaptive weight into the search phase of the algorithm can further enhance the WOA's search capability. The global search performance of the algorithm is stronger when the value of the inertia weight is larger, and the local search performance of the algorithm is stronger when the value of the inertia weight is smaller. Therefore, the global and local search capabilities are dynamically adjusted by applying a nonlinearly varying inertia weight with an increasing number of iterations. At the same time, the convergence speed of the algorithm is accelerated, and the optimization-seeking accuracy is tuned by drawing on the variation formula of the travel factor, as described in the previous section. The expressions are shown in Equations (22)–(25).

$$X(t_{iter} + 1) = X^*(t_{iter}) - \omega \cdot A \cdot D, p < 0.5, |A| < 1 \quad (22)$$

$$X(t_{iter} + 1) = X_{rand}(t_{iter}) - \omega \cdot A \cdot D'', p < 0.5, |A| \geq 1 \quad (23)$$

$$X(t_{iter} + 1) = \omega \cdot D' \cdot e^{br} \cdot \cos(2\pi r) + X^*(t_{iter}), p \geq 0.5 \quad (24)$$

$$\omega = 1 - 2 \left(\frac{t_{iter}}{T_{max}} \right)^3 \quad (25)$$

The parameters in Equations (22)–(24) are defined the same as those defined in Equations (17)–(19), except the ω . The value of t at the beginning of the number of iterations is smaller, while the weight ω and the adjustment step of the algorithm are larger; thus, the whale can search for the optimal solution in a larger area. As the number of iterations t increases, the weight ω becomes smaller, as does the adjustment step of the algorithm. At this time, the whales search more carefully in the optimal solution domain space. Therefore, ω changes adaptively with the current population's number of iterations, improving the WOA's search accuracy and accelerating its convergence speed. The probability of finding food also increases accordingly.

Moreover, Levy's distribution is a probability distribution proposed by the famous French mathematician Levy. There are many flying animals in nature whose flight paths follow Levy's distribution. Based on Levy's distribution, Levy's flight was created. It is a kind of flight mode with short and long steps. This random flight pattern makes the trajectory of flying animals more extensive, and the probability of finding food increases accordingly. The introduction of Levy flight trajectory for the position update formula is shown in Equation (26).

$$X(t_{iter} + 1) = X(t_{iter}) + \alpha \oplus Levy(\beta) \oplus X(t_{iter}) \quad (26)$$

where α is the step scale factor, taken as 0.01; $Levy(\beta)$ represents a random number subject to the Levy distribution with parameter β . $Levy(\beta)$ is defined by Equation (27). Where u and v are normally distributed; β taken as 1.5.

$$\begin{cases} Levy(\beta) \sim \frac{u}{|v|^{\frac{1}{\beta}}} \\ u \sim N(0, \sigma_u^2), v \sim N(0, \sigma_v^2) \\ \sigma_u = \left[\frac{\Gamma(1+\beta) \cdot \sin\left(\frac{\beta\pi}{2}\right)}{\Gamma\left(\frac{1+\beta}{2}\right) \cdot \beta \cdot 2^{\frac{\beta-1}{2}}}\right]^{\frac{1}{\beta}}, \sigma_v = 1 \end{cases} \quad (27)$$

The pseudo-code of IWOA is summarized in Algorithm 1.

Algorithm 1 Pseudo-code of IWOA

```

1: Initialize the whales population  $X_i(i = 1, 2, 3, \dots, N)$ 
2: Calculate the fitness of each search agent
3: Update  $X^*$  if there is a better solution
4:  $t = 1$ 
5: while  $t <$  maximum number of iterations do
6:   for each search agent do
7:     Update  $a, A, C, r_1, r_2$  and  $p$ 
8:     if  $p < 0.5$  then
9:       if  $|A| < 1$  then
10:        Update the position of search agent by the Equation (22)
11:       else if  $|A| \geq 1$  then
12:        Update the position of search agent by the Equation (23)
13:       end if
14:     else if  $p > 0.5$  then
15:       Update the position of the search agent by the Equation (24)
16:     end if
17:   end for
18:   Update the position of the search agent by the Equation (26)
19:   Check if any search agent goes beyond the search space and amend it
20:   Update  $X^*$  if there is a better solution
21:    $t = t + 1$ 
22:   return  $X^*$ 
23: end while

```

3.3. Testing Function Results

This subsection verifies the performance of the proposed method of the IWOA. Using eight selected testing functions from CEC2017 [38] to test the IWOA's performance. The experimental testing results of the IWOA are compared with the GA [39], PSO [40], WHO [41], WOA, and EWOA [42]. Table 1 depicts the average outcomes of the IWOA for 8 selected testing functions compared with the WOA, WOA based on adaptive weight strategy (AWOA), and WOA based on Levy flight trajectory (Levy-WOA), respectively.

Figures 4–7 show the convergence curves of the IWOA compared with the WOA, AWOA, and Levy-WOA on each right side of the subplots. They also show the function view spaces of the $F_3(x)$, $F_4(x)$, $F_5(x)$, and $F_9(x)$ from CEC2017 on each left side of the subplots.

Table 1. Comparison of average outcomes of the IWOA for 8 selected testing functions with the WOA, AWOA, and Levy-WOA.

Algorithms	WOA	AWOA	Levy-WOA	IWOA
$F_1(x)$	2.31×10^{-14}	4.39×10^{-13}	2.45×10^{-54}	1.81×10^{-59}
$F_2(x)$	5.77×10^{-25}	1.09×10^{-26}	6.83×10^{-59}	6.18×10^{-63}
$F_3(x)$	6.55×10^1	3.25×10^1	2.19×10^1	1.58×10^1
$F_4(x)$	2.23×10^2	1.92×10^2	1.80×10^2	1.81×10^2
$F_5(x)$	2.03×10^{-2}	3.16×10^{-11}	1.56×10^{-8}	2.70×10^{-12}
$F_9(x)$	3.51×10^{-2}	4.39×10^{-7}	2.45×10^{-9}	3.46×10^{-9}
$F_{11}(x)$	4.24×10^{-1}	4.53×10^{-3}	1.25×10^{-3}	3.33×10^{-4}
$F_{13}(x)$	9.85×10^0	6.10×10^0	2.40×10^0	4.06×10^0

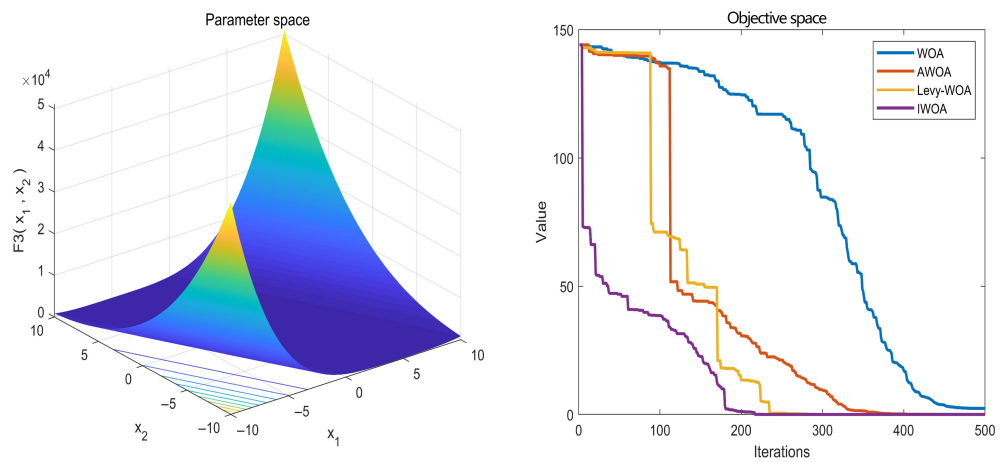


Figure 4. The evaluated experimental results of $F_3(x)$.

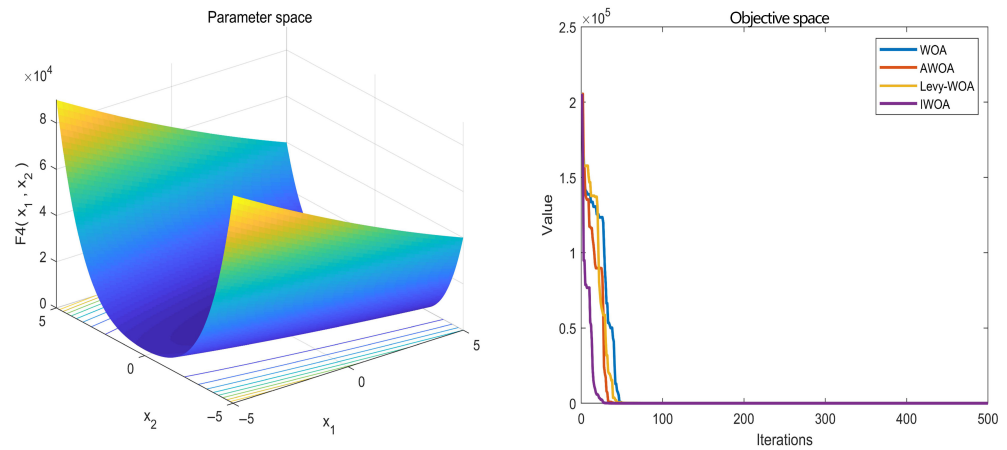


Figure 5. The evaluated experimental results of $F_4(x)$

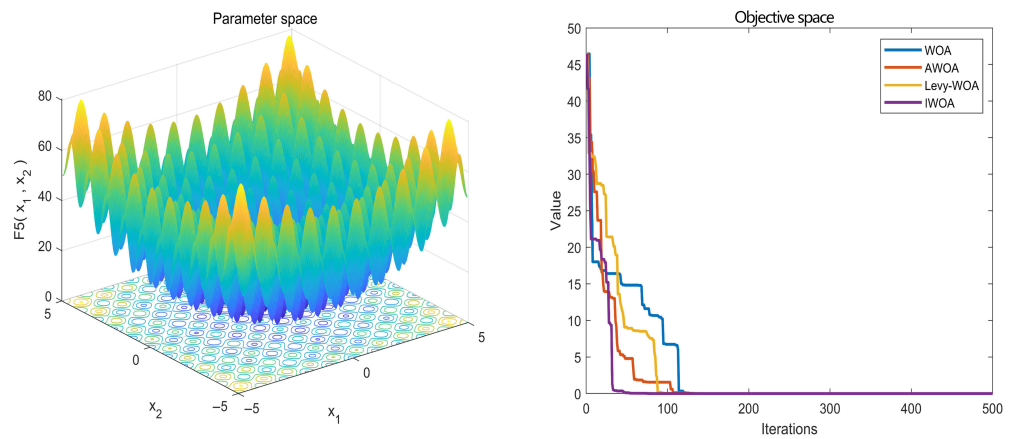


Figure 6. The evaluated experimental results of $F_5(x)$.

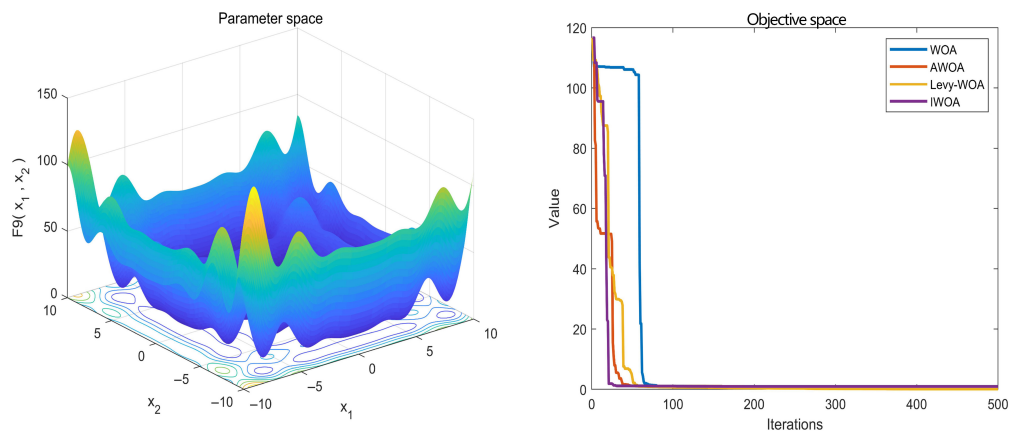


Figure 7. The evaluated experimental results of $F_9(x)$.

The curve of the convergence of the IWOA observed in Figures 4–7 shows that the fast one against the other algorithms belongs to the IWOA. It means that the convergence rate of the IWOA is quick to find out the global optimization. Table 2 depicts the comparison of the IWOA obtained results with the in pair compared to other algorithms in the literature.

Table 2. The obtained average results of the IWOA for the selected testing functions are compared with the GA, PSO, WHO, and E-WOA.

Algorithms	GA	PSO	WHO	EWOA	IWOA
$F_1(x)$	6.92×10^{-4}	5.38×10^{-11}	6.89×10^{-57}	3.56×10^{-50}	1.81×10^{-59}
$F_2(x)$	4.84×19^{-9}	9.27×10^{-23}	1.74×10^{-61}	5.72×10^{-55}	6.18×10^{-63}
$F_3(x)$	1.08×10^2	7.50×10^1	1.44×10^1	2.37×10^1	1.58×10^1
$F_4(x)$	3.28×10^2	2.13×10^2	1.67×10^2	1.87×10^2	1.81×10^2
$F_5(x)$	8.39×10^{-2}	3.23×10^{-2}	4.48×10^{-9}	2.39×10^{-11}	2.70×10^{-12}
$F_9(x)$	1.18×10^{-1}	7.46×10^{-2}	2.23×10^{-8}	7.14×10^{-8}	3.46×10^{-9}
$F_{11}(x)$	3.72×10^0	4.02×10^{-1}	7.07×10^{-4}	3.92×10^{-3}	3.33×10^{-4}
$F_{13}(x)$	2.39×10^1	1.25×10^1	4.93×10^0	4.76×10^0	4.06×10^0

Table 2 shows the experimental data of the obtained results of the IWOA compared with the other methods. It can be seen that the IWOA produces the optimization results of functions, e.g., $F_1(x)$, $F_2(x)$, $F_5(x)$, $F_9(x)$, $F_{11}(x)$, and $F_{13}(x)$ better than the other algorithms in terms of the optimization accuracy, and the optimization results of all testing functions of IWOA are improved compared with the original algorithm.

4. Analysis of Calculation Cases

This section studies a low-voltage grid-connected microgrid system composed of dispatchable and non-dispatchable distributed generation units; its optimal operations planning problem was solved and analyzed by the IWOA. The dispatchable distributed generation units included fossil fuel generators, batteries, and a large grid. The non-dispatchable distributed generation units were renewable energy sources whose power output could be controlled or dispatched. The structure of this low-voltage grid-connected microgrid system is shown in Figure 8.

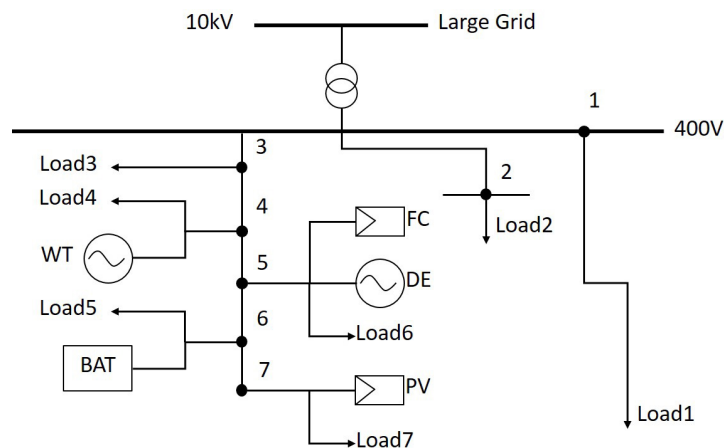


Figure 8. The structure of a low-voltage grid-connected microgrid system.

4.1. Relevant Arithmetic Data

According to the datasets given by [43,44], based on the real-time wind speed, ambient temperature, and light intensity, combined with the mathematical model mentioned above, the 24-h electricity load, PV, and WT output data for a typical day in summer at some sites are shown in Figure 9.

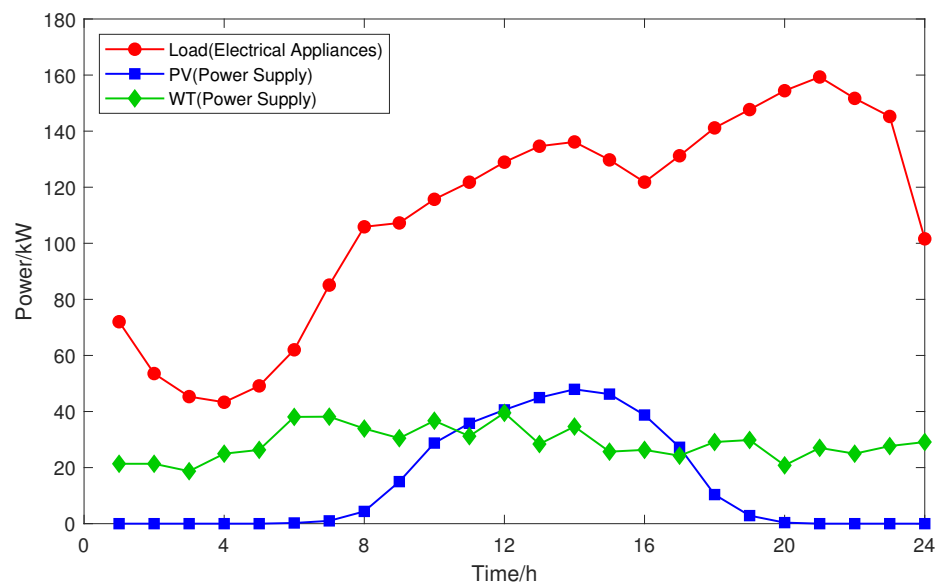


Figure 9. Fixed loads and power outputs from non-dispatchable generators.

According to the time-sharing tariff and renewable energy feed-in tariff, the peak hours were 10:00–15:00 and 18:00–21:00; the weekdays were 07:00–10:00, 15:00–18:00, and 21:00–23:00; and the valley hours were 23:00–07:00. The purchase and sale prices for each period time are shown in Table 3. The parameters, such as upper and lower limits of power

output and O&M costs of DERs in the microgrid, are shown in Table 4. The parameters related to the SOC of the battery are shown in Table 5. The pollutant emissions factors during the operation of the FC and DE in the microgrid are shown in Table 6.

Table 3. Market price of electricity [45].

Types	Price/[\$·(kWh) ⁻¹]		
	Peak Period	Normal Period	Through Period
Buy	0.84	0.51	0.19
Sell	0.42	0.26	0.09

Table 4. Generation parameters of each DER in microgrid [45].

Types	Minimum Power/(kW)	Maximum Power/(kW)	Maintenance Costs/(\$/kW)	Climb Rates/(kW/min)
WT	0	40	0.036	/
PV	0	50	0.012	/
FC	5	60	0.107	2
DE	6	80	0.205	3
BAT	−30	30	0.005	/
Grid	−60	60	0.001	/

Table 5. Battery charge-discharge parameters [46].

Parameters	Value
Charge-discharge efficiency	0.9
Self loss rate	0.01
Maximum charge-discharge power/kW	30
Maximum state of charge	0.9
Minimum state of charge	0.2
Initial state of charge	0.6

Table 6. Pollutant emission factors for each DER in the microgrid.

Types of Pollutant	Converted Costs/(\$/kg)	Emission Factors/(kg/kWh)	
		DE	FC
CO ₂	0.0052	0.542	0.635
SO ₂	0.693	0	0
NO _x	1.19	3.1×10^{-5}	2.3×10^{-5}
CO	0.201	6.5×10^{-5}	5.4×10^{-5}

4.2. Analysis of Optimization Results of Grid-Connected Operation

In grid-connected operation, microgrid load is provided by DERs, which purchase power from the large grid to compensate for load demands whenever microgrid power output is insufficient. Moreover, the microgrid sells power to the large grid, to subsidize generation costs whenever its power output is a surplus.

Figure 10 shows the output power of DERs other than PVs and WTs, and the purchased and sold power that is generated by interactions with the large grid, after optimization using the IWOA. Figure 11 shows the generation share of each DER in the day-ahead dispatch.

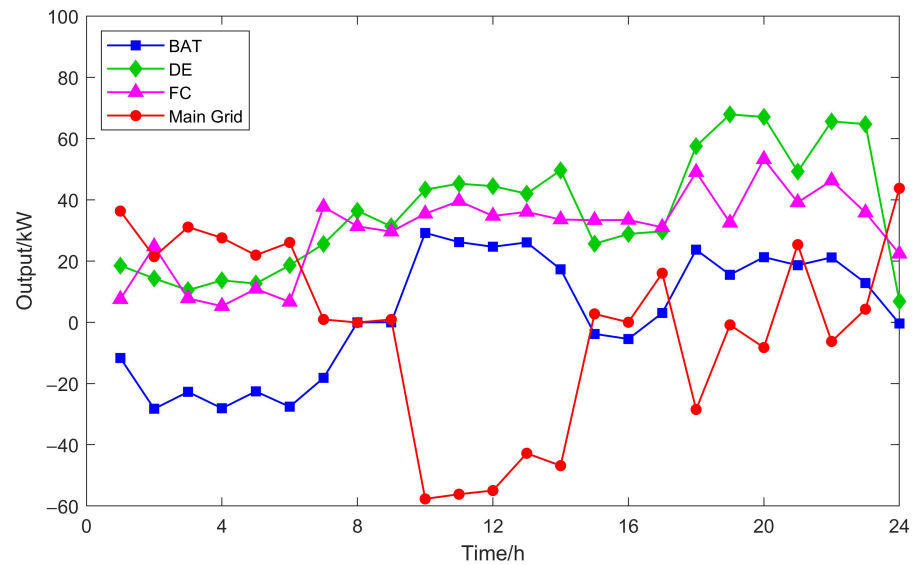


Figure 10. The outputs of each DER in microgrid under grid-connected operation by running IWOA.

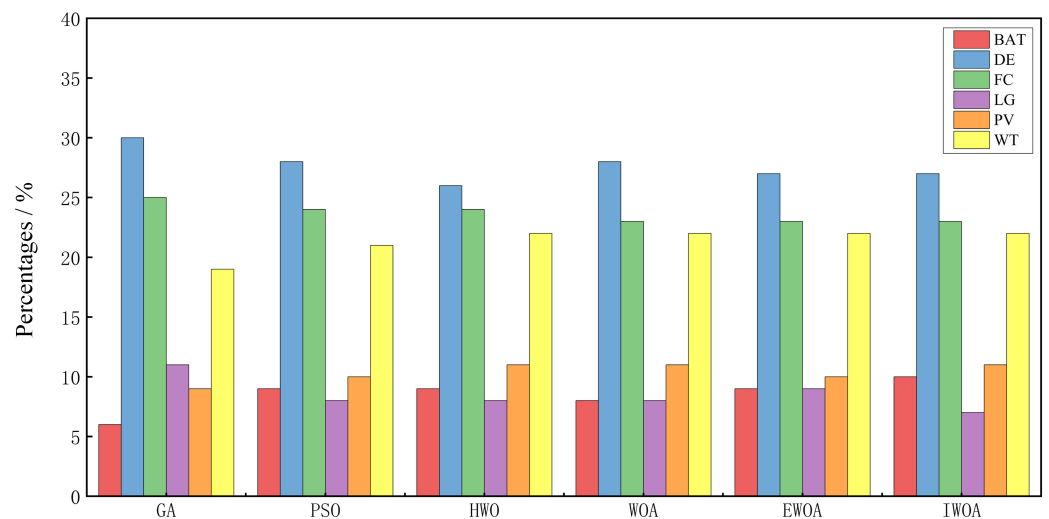


Figure 11. Percentages of outputs from each DER by running GA, PSO, WHO, WOA, EWOA, and IWOA.

From Figure 10, we can see that from 00:00 to 07:00, microgrid load demand was reduced, and the large grid was in the valley. The price of purchasing electricity from the large grid was lower than the price of using DE and FC generation. Thus, the BAT was charged as much as possible while meeting the load demand. From 07:00 to 10:00, the large grid was in the normal period, and the price of purchasing and selling electricity from the large grid was not much different from the price of DE and FC generation. Thus, the system adjusted the output of the DE, FC, and BAT according to the load demand.

From 10:00 to 15:00, the load demand increased further, and it was during the peak time of the large grid; the price of selling electricity to the grid was higher than the price of using the DE and FC. PV output reached peak range at this time, and the system increased the output of the BAT while selling surplus power to the large grid, to generate more subsidies for its generation costs. From 15:00 to 18:00, the large grid was in the normal period and the PV output began to decrease; the microgrid reduced the power sold to the large grid, adjusted the DE and FC output, and charged the BAT.

From 18:00 to 21:00, the peak time of the whole day, the large grid was in the peak period. During this time, the PV basically stopped generating power, and the DE, FC, and

BAT were all at high generation levels; thus, when the load demand was met, the power was sold to the large grid as much as possible. If the DERs still did not meet the load demand, the microgrid made up for this by purchasing power from the large grid.

From 21:00 to 24:00, the large grid was in the normal period, and the load demand began to decrease. Thus, the system reduced the power output of the BAT and changed the power output of the DE, FC, and BAT, as well as the power purchased and sold by the large grid, according to the load demand.

From Figure 11, we can see that by running IWOA, the WT and PV accounted for about one-third of the total power generation in an entire day; meanwhile, the microgrid purchased about 7% of the power from the large grid, the BAT discharged about 10%, and DE and FC generation accounted for about 50%. From the perspective of microgrid self-sufficiency, the system was less dependent on the large grid and operated more stably.

To verify the improvement of the IWOA, the model solution was compared with the GA, PSO, WOA, WHO, and the EWOA, which were all run 10 times, with the average values selected for analysis. Using the objective function given by Equation (1), the worst fitness curves obtained by running each algorithm 10 times are shown in Figure 12, and the best fitness curves obtained by running each algorithm 10 times are shown in Figure 13. The worst, best, and average objective function fitness values, which were obtained after 10 runs of each algorithm, are shown in Table 7.

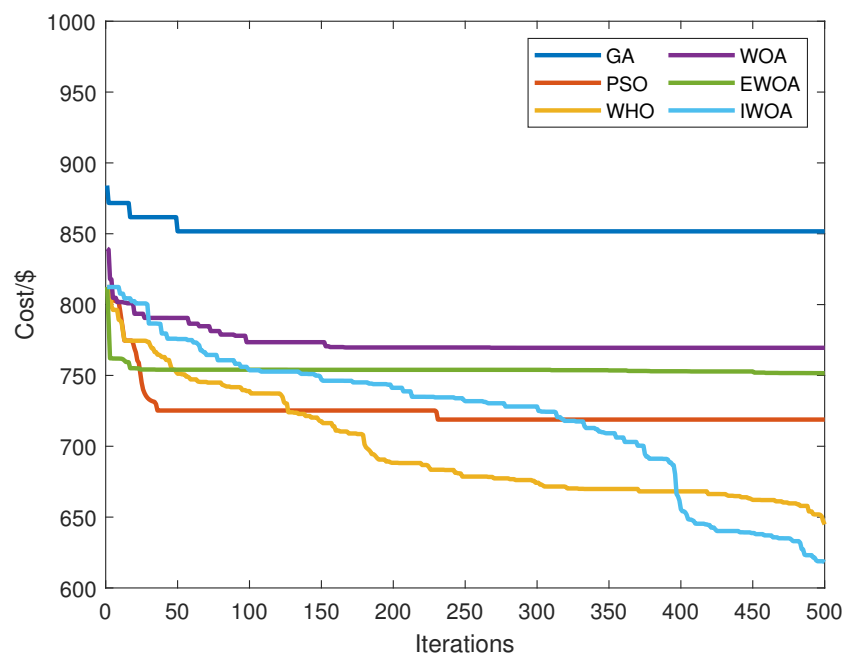


Figure 12. The worst operation cost curves of microgrid obtained by running GA, PSO, WHO, WOA, EWOA, and IWOA.

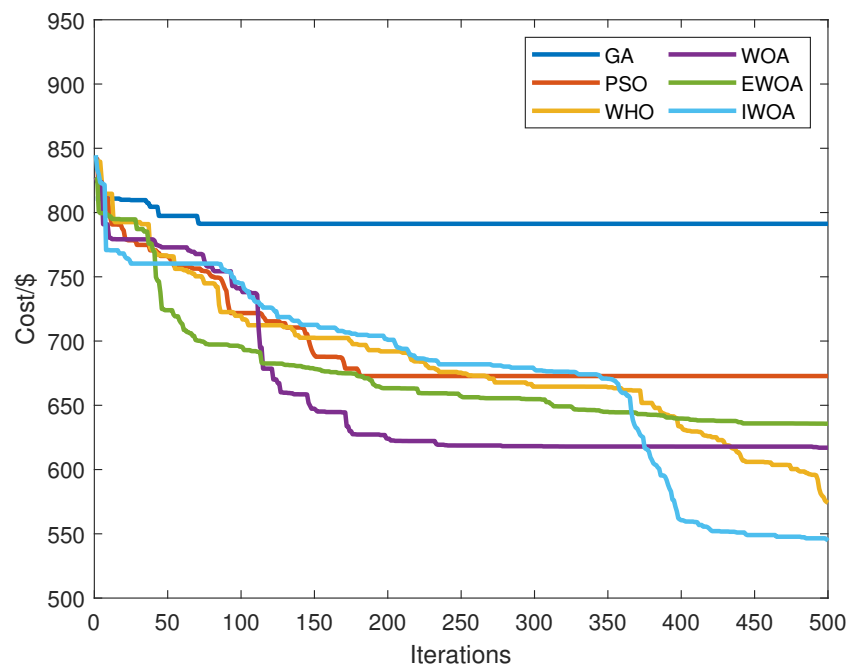


Figure 13. The best operation cost curves of microgrid obtained by running GA, PSO, WHO, WOA, EWOA, and IWOA.

Table 7. The worst, best, and average of each algorithm run after 10 runs, respectively.

Types of Algorithm	Cost/\$		
	Worst Fitness	Average Fitness	Best Fitness
GA	851.6949	822.3026	791.2397
PSO	718.8405	703.6297	672.7780
WHO	644.8292	608.6623	574.1178
WOA	769.5022	691.2630	616.9936
EWOA	751.5720	686.7476	635.6775
IWOA	618.1832	580.8272	544.6443

Figure 11 shows that compared with the GA, PSO, WHO, WOA, and the WOA, the calculated microgrid–large grid interactions are lower by about 4%, 1%, 1%, 1%, and 2%, respectively; moreover, Table 7 shows that compared with the GA, PSO, WHO, WOA, and the EWOA, the average cost of the IWOA calculation is lower by about 29%, 17%, 5%, 16%, and 15%, respectively. The results indicate that the IWOA proposed in this paper has good optimization-seeking accuracy, which works well for solving the optimal operations planning problem of this grid-connected microgrid.

5. Conclusions

In this study, a grid-connected microgrid generating model containing WT, PV, DE, FC, and BAT was established with minimized operation costs as the objective function to reduce microgrid pollution emissions. To better address this issue, an improved whale algorithm based on adaptive weight strategy and Levy flight trajectory was proposed, which further reduced the operating costs of the grid-connected microgrid. Using IWOA, the output ratio of RESs increased, and the microgrid purchased less power from the large grid. Moreover, with BAT as a power storage system and participating in coordinated control, the quality of the microgrid power supply was effectively adjusted by BAT, which guaranteed the symmetry in renewable energy and microgrid system.

In analyzing the output ratio of each DER to gross generation, the output ratio of each DER calculated by IWOA was compared with that calculated by GA, PSO, WHO, WOA, and EWOA. The results showed that the microgrid operations planning problems

solved by IWOA is more effective in enhancing the independence of microgrid operations. The increased ratio of RESs also further improved the environmental friendliness of the microgrid. Moreover, in the scenario where the market price of electricity was considered, the objective function was solved by GA, PSO, WHO, WOA, EWOA, and IWOA, and the calculated results represented the operation costs. A comparison of the average operation costs after running each algorithm ten independent times has been presented to prove the capability of the IWOA proposed in this paper is better for solving microgrid operations planning problems, which further reduces the microgrid operation costs and has good application prospects.

Author Contributions: Conceptualization, methodology, and software, Y.L.; validation and formal analysis, Y.L. and S.Y.; writing—original draft preparation, Y.L. and D.L.; writing—review and editing, D.L.; visualization and supervision, S.Z. All authors have read and agreed to the published version of the manuscript.

Funding: This research received no external funding.

Institutional Review Board Statement: Not applicable.

Informed Consent Statement: Not applicable.

Data Availability Statement: Not applicable.

Conflicts of Interest: The authors declare no conflict of interest.

List of Symbols

t	Index representing time
T	Time period
$C_{grid}(t)$	The cost of microgrid interaction with the large grid
$C_{BE}(t), C_{WT}(t), C_{PV}(t)$	The maintenance costs of BAT, WT, PV
$C_{DE}(t), C_{FC}(t)$	The maintenance costs of DE, FC
$E_{CO_2}^{DE}, E_{SO_2}^{DE}, E_{NO_x}^{DE}, E_{CO}^{DE}$	The converted costs of various pollutants generated by DE
$E_{CO_2}^{FC}, E_{SO_2}^{FC}, E_{NO_x}^{FC}, E_{CO}^{FC}$	The converted costs of various pollutants generated by FC
$P_{grid}(t)$	The power of microgrid interaction with the large grid
$P_{WT}(t), P_{PV}(t), P_{DE}(t), P_{FC}(t)$	Power generation of WT, PV, DE, FC at time t
t_{iter}	Index representing current iterations of the algorithm
T_{max}	Index representing maximum number of algorithm iterations

References

1. Wang, K.; Yu, J.; Yu, Y.; Qian, Y.; Zeng, D.; Guo, S.; Xiang, Y.; Wu, J. A survey on energy internet: Architecture, approach, and emerging technologies. *IEEE Syst. J.* **2017**, *12*, 2403–2416. [[CrossRef](#)]
2. Ismael, S.M.; Aleem, S.H.A.; Abdelaziz, A.Y.; Zobaa, A.F. State-of-the-art of hosting capacity in modern power systems with distributed generation. *Renew. Energy* **2019**, *130*, 1002–1020. [[CrossRef](#)]
3. Adinolfi, G.; Cigolotti, V.; Graditi, G.; Ferruzzi, G. Grid integration of distributed energy resources: Technologies, potentials contributions and future prospects. In Proceedings of the 2013 International Conference on Clean Electrical Power (ICCEP), IEEE, Alghero, Italy, 11–13 June 2013; pp. 509–515. [[CrossRef](#)]
4. Ghasemi, A.; Enayatzare, M. Optimal energy management of a renewable-based isolated microgrid with pumped-storage unit and demand response. *Renew. Energy* **2018**, *123*, 460–474. [[CrossRef](#)]
5. Zia, M.F.; Elbouchikhi, E.; Benbouzid, M. Microgrids energy management systems: A critical review on methods, solutions, and prospects. *Appl. Energy* **2018**, *222*, 1033–1055. [[CrossRef](#)]
6. Mengelkamp, E.; Gärtner, J.; Rock, K.; Kessler, S.; Orsini, L.; Weinhardt, C. Designing microgrid energy markets: A case study: The Brooklyn Microgrid. *Appl. Energy* **2018**, *210*, 870–880. [[CrossRef](#)]
7. Samad, T.; Annaswamy, A.M. Controls for smart grids: Architectures and applications. *Proc. IEEE* **2017**, *105*, 2244–2261. [[CrossRef](#)]
8. Strunz, K.; Abbasi, E.; Huu, D.N. DC microgrid for wind and solar power integration. *IEEE J. Emerg. Sel. Top. Power Electron.* **2014**, *2*, 115–126. [[CrossRef](#)]
9. Kaur, A.; Kaushal, J.; Basak, P. A review on microgrid central controller. *Renew. Sustain. Energy Rev.* **2016**, *55*, 338–345. [[CrossRef](#)]

10. Ngo, T.G.; Nguyen, T.T.T.; Nguyen, T.X.H.; Nguyen, T.D.; Do, V.C. A solution to power load distribution based on enhancing swarm optimization. In Proceedings of the International Conference on Engineering Research and Applications (ICERA), Springer, Thai Nguyen, Vietnam, 1–2 December 2020; pp. 53–63. [\[CrossRef\]](#)
11. Liu, H.; Liu, W. The analysis of effects of clean energy power generation. In Proceedings of the Applied Energy Symposium and Forum; Low-Carbon Cities and Urban Energy Systems (CUE), Shanghai, China, 5–7 June 2018; pp. 947–952. [\[CrossRef\]](#)
12. Nguyen, T.T.; Ngo, T.G.; Dao, T.K.; Nguyen, T.T.T. Microgrid operations planning based on improving the flying sparrow search algorithm. *Symmetry* **2022**, *14*, 168. [\[CrossRef\]](#)
13. Baziar, A.; Kavousi-Fard, A. Considering uncertainty in the optimal energy management of renewable micro-grids including storage devices. *Renew. Energy* **2013**, *59*, 158–166. [\[CrossRef\]](#)
14. Wang, M.J.; Pan, J.S.; Dao, T.k.; Ngo, T.G. A load economic dispatch based on ion motion optimization algorithm. In *Advances in Intelligent Information Hiding and Multimedia Signal Processing*; Springer: Singapore, 2020; pp. 115–125. [\[CrossRef\]](#)
15. Pan, J.S.; Liu, N.; Chu, S.C. A hybrid differential evolution algorithm and its application in unmanned combat aerial vehicle path planning. *IEEE Access* **2020**, *8*, 17691–17712. [\[CrossRef\]](#)
16. Abdel-Basset, M.; Abdel-Fatah, L.; Sangaiah, A.K. Metaheuristic algorithms: A comprehensive review. In *Computational Intelligence for Multimedia Big Data on the Cloud with Engineering Applications*; Arun, K.S., Michael, S., Zhiyong, Z., Eds.; Elsevier: Amsterdam, The Netherlands, 2018; pp. 185–231.
17. Bahmani-Firouzi, B.; Azizipناه-Abarghoee, R. Optimal sizing of battery energy storage for micro-grid operation management using a new improved bat algorithm. *Int. J. Electr. Power Energy Syst.* **2014**, *56*, 42–54. [\[CrossRef\]](#)
18. Mahmoud, M.M.; Khalid Ratib, M.; Aly, M.M.; Abdel-Rahim, A.M.M. Wind-driven permanent magnet synchronous generators connected to a power grid: Existing perspective and future aspects. *Wind. Eng.* **2022**, *46*, 189–199. [\[CrossRef\]](#)
19. Abbasi, B.Z.; Javaid, S.; Bibi, S.; Khan, M.; Malik, M.N.; Butt, A.A.; Javaid, N. Demand side management in smart grid by using flower pollination algorithm and genetic algorithm. In Proceedings of the 12th International Conference on P2P, Parallel, Grid, Cloud and Internet Computing (3PGCIC), Barcelona, Spain, 8–10 November 2017; pp. 424–436. [\[CrossRef\]](#)
20. Zhang, J.; Wu, Y.; Guo, Y.; Wang, B.; Wang, H.; Liu, H. A hybrid harmony search algorithm with differential evolution for day-ahead scheduling problem of a microgrid with consideration of power flow constraints. *Appl. Energy* **2016**, *183*, 791–804. [\[CrossRef\]](#)
21. Rasheed, M.B.; Javaid, N.; Ahmad, A.; Awais, M.; Khan, Z.A.; Qasim, U.; Alrajeh, N. Priority and delay constrained demand side management in real-time price environment with renewable energy source. *Int. J. Energy Res.* **2016**, *40*, 2002–2021. [\[CrossRef\]](#)
22. Sukumar, S.; Mokhlis, H.; Mekhilef, S.; Naidu, K.; Karimi, M. Mix-mode energy management strategy and battery sizing for economic operation of grid-tied microgrid. *Energy* **2017**, *118*, 1322–1333. [\[CrossRef\]](#)
23. Askarzadeh, A. A memory-based genetic algorithm for optimization of power generation in a microgrid. *IEEE Trans. Sustain. Energy* **2018**, *9*, 1081–1089. [\[CrossRef\]](#)
24. Gholami, K.; Dehnavi, E. A modified particle swarm optimization algorithm for scheduling renewable generation in a micro-grid under load uncertainty. *Appl. Soft Comput.* **2019**, *78*, 496–514. [\[CrossRef\]](#)
25. Nadimi-Shahraki, M.H.; Fatahi, A.; Zamani, H.; Mirjalili, S.; Oliva, D. Hybridizing of Whale and Moth-Flame Optimization Algorithms to Solve Diverse Scales of Optimal Power Flow Problem. *Electronics* **2022**, *11*, 831. [\[CrossRef\]](#)
26. Lahon, R.; Gupta, C.P.; Fernandez, E. Priority-based scheduling of energy exchanges between cooperative microgrids in risk-averse environment. *IEEE Syst. J.* **2020**, *14*, 1098–1108. [\[CrossRef\]](#)
27. Lahon, R.; Gupta, C.P. Risk-based coalition of cooperative microgrids in electricity market environment. *IET Gener. Transm. Distrib.* **2018**, *12*, 3230–3241. [\[CrossRef\]](#)
28. Lahon, R.; Gupta, C.P.; Fernandez, E. Optimal power scheduling of cooperative microgrids in electricity market environment. *IEEE Trans. Industr. Inform.* **2019**, *15*, 4152–4163. [\[CrossRef\]](#)
29. Trivedi, I.N.; Jangir, P.; Bhoje, M.; Jangir, N. An economic load dispatch and multiple environmental dispatch problem solution with microgrids using interior search algorithm. *Neural Comput. Appl.* **2018**, *30*, 2173–2189. [\[CrossRef\]](#)
30. Motevasel, M.; Seifi, A.R. Expert energy management of a micro-grid considering wind energy uncertainty. *Energy Convers. Manag.* **2014**, *83*, 58–72. [\[CrossRef\]](#)
31. Tahmasebi, M.; Pasupuleti, J.; Mohamadian, F.; Shakeri, M.; Guerrero, J.M.; Basir Khan, M.R.; Nazir, M.S.; Safari, A.; Bazmohammadi, N. Optimal operation of stand-alone microgrid considering emission issues and demand response program using whale optimization algorithm. *Sustainability* **2021**, *13*, 7710. [\[CrossRef\]](#)
32. Khodaei, A. Provisional microgrids. *IEEE Trans. Smart Grid* **2015**, *6*, 1107–1115. [\[CrossRef\]](#)
33. Khodaei, A. Provisional microgrid planning. *IEEE Trans. Smart Grid* **2017**, *8*, 1096–1104. [\[CrossRef\]](#)
34. Aghajani, G.; Shayanfar, H.; Shayeghi, H. Demand side management in a smart micro-grid in the presence of renewable generation and demand response. *Energy* **2017**, *126*, 622–637. [\[CrossRef\]](#)
35. Luo, L.; Abdulkareem, S.S.; Rezvani, A.; Miveh, M.R.; Samad, S.; Aljojo, N.; Pazhoohesh, M. Optimal scheduling of a renewable based microgrid considering photovoltaic system and battery energy storage under uncertainty. *J. Energy Storage* **2020**, *28*, 101306. [\[CrossRef\]](#)
36. Mirjalili, S.; Lewis, A. The whale optimization algorithm. *Adv. Eng. Softw.* **2016**, *95*, 51–67. [\[CrossRef\]](#)
37. Zhang, J.; Wang, J.S. Improved whale optimization algorithm based on nonlinear adaptive weight and golden sine operator. *IEEE Access* **2020**, *8*, 77013–77048. [\[CrossRef\]](#)

38. Wu, G.; Mallipeddi, R.; Suganthan, P.N. *Problem Definitions and Evaluation Criteria for the CEC 2017 Competition on Constrained Real-Parameter Optimization*; Technical Report; National University of Defense Technology: Changsha, China; Kyungpook National University: Daegu, Korea; Nanyang Technological University: Singapore, 2017.
39. Whitley, D. A genetic algorithm tutorial. *Stat. Comput.* **1994**, *4*, 65–85. [[CrossRef](#)]
40. Kennedy, J.; Eberhart, R. Particle swarm optimization. In Proceedings of the ICNN'95-International Conference on Neural Networks, IEEE, Perth, WA, Australia, 27 November–1 December 1995; Volume 4, pp. 1942–1948.
41. Metwally Mahmoud, M. Improved current control loops in wind side converter with the support of wild horse optimizer for enhancing the dynamic performance of PMSG-based wind generation system. *Int. J. Model. Simul.* **2022**.
42. Qais, M.H.; Hasanien, H.M.; Alghuwainem, S. Enhanced whale optimization algorithm for maximum power point tracking of variable-speed wind generators. *Appl. Soft Comput.* **2020**, *86*, 105937. [[CrossRef](#)]
43. Seel, J.; Mills, A.; Millstein, D.; Gorman, W.; Jeong, S. Solar-to-Grid Public Data File for Utility-scale (UPV) and Distributed Photovoltaics (DPV) Generation, Capacity Credit, and Value. 2020. Available online: <https://data.openei.org/submissions/2881> (accessed on 30 November 2022).
44. Thibedeau, J. July 2014 Green Machine Florida Canyon Hourly Data. 2014. Available online: <https://gdr.openei.org/submissions/431> (accessed on 30 November 2022).
45. Nguyen, T.T.; Dao, T.K.; Nguyen, T.D. An Optimal Microgrid Operations Planning Using Improved Archimedes Optimization Algorithm. *IEEE Access* **2022**, *10*, 67940–67957. [[CrossRef](#)]
46. Zhang, Z.; Wang, Z.; Wang, H.; Zhang, H.; Yang, W.; Cao, R. Research on bi-level optimized operation strategy of microgrid cluster based on IABC algorithm. *IEEE Access* **2021**, *9*, 15520–15529. [[CrossRef](#)]

Disclaimer/Publisher's Note: The statements, opinions and data contained in all publications are solely those of the individual author(s) and contributor(s) and not of MDPI and/or the editor(s). MDPI and/or the editor(s) disclaim responsibility for any injury to people or property resulting from any ideas, methods, instructions or products referred to in the content.